MGII QUASAR ABSORPTION LINE SYSTEMS AS A PROBE OF GALAXY STRUCTURAL AND KINEMATIC EVOLUTION

Jessica L. Evans[1]

[1] *New Mexico State University, Department of Astronomy, P.O. Box 30001, MSC 4500, Las Cruces, New Mexico 88003, jlevans@nmsu.edu*

ABSTRACT

Armed with the largest database of high resolution, high signal-to-noise quasar absorption line spectra ever compiled, I propose to analyze the sample of $\sim$ 360 Mg II $\lambda\lambda 2796, 2803$ doublet systems in order to shed much needed light on our current picture of galaxy and intergalactic medium gas kinematics and structure, and to chart how these have changed throughout cosmic time. This will be achieved by studying the distributions of, and evolution in, the system equivalent widths, column densities, Doppler b parameters, flux decrements, and velocity widths over the redshift range $0.2 < z < 2.6$ in order to construct a statistical framework for understanding the physical processes selected by the presence of Mg II. Additionally, with the aid of powerful cosmological hydrodynamic n-body simulations, I will use synthetic quasar lines of sight to place constraints on scenarios of galaxy formation. In turn I will be able to study Mg II selected "galaxies" as has never been done before in such great detail at such high redshifts.

1. INTRODUCTION

Our current understanding of galaxy formation and evolution is still far from complete. We would like a more comprehensive picture of the structure and kinematics of galaxy gas and the intergalactic medium (IGM). Quasar absorption line spectra are an extremely useful means of building up statistics for constraining the various scenarios of metal enrichment, inflow and outflow, ionization conditions, gas kinematics, and gas structure.

The resonant Mg II $\lambda\lambda 2796, 2803$ doublet is a particularly important feature in quasar absorption line spectra. Studies of Mg II absorption have revealed information about a plethora of galactic environments. In their analysis of Mg II systems with $W_r(2796) > 1.8$ Å, Bond et al. (2001a,b) favored expanding superbubbles as the process accounting for a substantial

fraction of this equivalent width regime. Steidel et al. (1994) concluded that strong Mg II absorbers (defined as having $W_r(2796) \geq 0.3$ Å) were typically originating in normal luminous galaxies, while Churchill et al. (1999) suggested that some fraction of weak Mg II absorption (i.e. $W_r(2796) < 0.3$ Å) might also arise in dwarf or low surface brightness galaxies. Milutinović et al. (2006) used an ionization model to study weak Mg II absorption and concluded that filamentary and sheetlike geometries were likely, and that most of these absorbers were arising within the cosmic web in the vicinities of luminous galaxies. Photoionization modeling of weak Mg II systems with associated C IV led Lynch & Charlton (2007) to argue for a scenario of a shell geometry as might be expected for supernova remnants or high velocity clouds moving in a hot corona. Mg II absorbers can be used to study all of these structures in and around galaxies.

There is a wealth of information that can be extracted from a survey of Mg II absorption lines. One of the main results of previous Mg II absorption line studies is that the strongest Mg II absorbers ($W_r(2796) > 1.0$ Å) exhibit the most pronounced redshift evolution (Steidel & Sargent 1992; Nestor et al. 2005) in the sense that their numbers per unit redshift are evolving away. The moderate equivalent width systems ($0.3 < W_r(2796) < 1.0$ Å) do not seem to exhibit this evolution, implying that there are two distinct phenomena giving rise to the absorption.

The evolution in the strongest systems is one of the most intriguing topics of Mg II absorption. To determine the physical cause of the decrease in the number of these systems having equivalent widths greater than $\sim$ 1.0 Å, two possible scenarios must be explored. One factor that could cause the absorber strengths to decrease is a decrease in the column densities of system components; this would mean either a decrease in the gas masses of the clouds or a change in the ionizaton conditions to disfavor Mg II. The other possible factor is a decrease in the average kinematic spreads of the systems - i.e., the Mg II absorbing gas might still be present in comparable quantities, but has become kinematically less active or complex, and the system components have become more aligned in velocity space. By using our large statistical database of spectra, I plan to explore these two effects and determine their relative contributions to the equivalent width evolution. This can be achieved using Voigt profile (VP) modeling to decompose systems into their components and extracting the number of components as well as their column densities, velocities, and Doppler b parameters. In addition I will study the distributions of flux decrements per pixel, which provide excellent statistics in looking at the relative optical depths of absorption systems. The kinematic characteristics of Mg II systems can be examined by using not only the VP component velocities to construct a two-point correlation function (see § 4.3), but also the velocity widths of systems, to determine the extent to which systems may be systematically becoming narrower over time. All of these distributions must be compared for various red-

shift bins and at various equivalent widths cutoffs in order to create a dynamical picture of Mg II selected structures.

Another area of intense interest in the study of Mg II absorbers is in the weak systems. Many of the earlier surveys did not have the spectral resolution or quality to study this equivalent width regime, and my project will constitute by far the largest sample of high resolution, high signal-to-noise spectra to date, which can probe what is expected to be the most tenuous outer regions of galaxies as well as IGM gas. By using three different techniques to measure the redshift sensitivity function $g(W_r, z)$ and thus the redshift number density, dN/dz (see § 4.4), I hope to obtain the most accurate measurements yet of the statistics of this important population of absorbers. Narayanan et al. (2007) found that dN/dz of weak Mg II absorbers peaks at $z = 1.2$ and decreases at higher redshifts. This may be due to changes in gas structure, ionization conditions, or blending effects whereby the weak systems are obscured by the presence of strong systems at high redshift.

Past studies have relied on extremely simple models or concepts of velocity structure as points of reference to which to compare the results of the data analyses (see e.g. Charlton & Churchill 1998; Steidel et al. 2002). Fortunately, we now have a powerful tool that will enable far more detailed analysis of galaxy kinematics in the context of quasar absorption lines: synthetic quasar lines of sight generated through cosmological hydrodynamic n-body simulations of galaxy formation and evolution. These simulations will not only allow for a more complete understanding, structurally and kinematically, of the environments we are observing in the normally pencil-beam, statistical nature of quasar absorption line work, but also in turn my comparisons of the simulated Mg II systems to the observations will place much needed constraints on the galaxy simulation parameters.

If systematic differences are found between the properties of the observed quasar absorption line spectra and those of the synthetic spectra, then the galaxy simulation code could be modified to more accurately reproduce the observations. The stellar feedback model might then have to be changed, since this a key to the galaxy formation and controls inflow, outflow, heating, and the synthesis of metals. The latter in turn determines the rate of radiative cooling. If these properties are not accurately simulated, then the temperature, density, and metallicity profiles with galactocentric distance will be incorrect. This will affect the distribution of Mg II and the covering factor (Steidel 1995; Tripp & Bowen 2005; Kacprzak et al. 2008). Another possibility is that the simulation resolution might have to be increased to reproduce the observed Mg II absorber population.

2. SCIENCE GOALS

I propose to use the statistical database of Mg II absorbers that we have compiled to explore the nature of the evolution of the gas giving rise to this absorption and of the galaxies that are associated with it. The quantities I will study fall into two groups. The first includes those that are extracted directly from the flux values in the spectra: (i) the equivalent widths; (ii) the flux decrements in each pixel; and (iii) the velocity widths. The second includes those that require VP modeling: (i) the column densities; (ii) the Doppler b parameters; (iii) the number of VP components in a system; and (iv) the velocity two-point correlation function, which is measured by taking into account all of the VP fit component velocities. By studying the equivalent width, column density, and other distributions down to the weakest observable systems, I hope to probe the interface of galaxies and the IGM. Analysis of quasar absorption line spectra allows more tenuous gas to be studied than would imaging alone. The goals of this project include:

1. Study the equivalent width and column density distributions of Mg II absorbers to see whether there is a turnover at small equivalent widths and what the implications are for gas halos.

2. Study the Doppler b parameter distribution to learn about the temperature and turbulence conditions of Mg II absorbing gas.

3. Use velocity information to explore the kinematics of Mg II selected galaxies. For instance, we can calculate the two-point velocity correlation function of components within systems, the velocity spread and the total velocity width. These quantities yield clues about the nature of the kinematics; they indicate the kinematic extent and structure of the gas, and may offer information on whether the systems are consistent with disk-like rotation, inflow, or outflow, for instance.

4. Analyze the distributions of flux decrements per pixel for different redshift bins, velocity bins, and at various equivalent width cutoffs to gain insight about the evolution of the absorbing gas. The flux decrement is useful because it is a measure of the optical depths of the systems. As an example, an observation of decreasing flux decrements within systems of similar equivalent width could be interpreted as clouds breaking up into smaller, optically thinner components in velocity.

5. Study the statistics of Mg II absorbers over the redshift range $0.2 < z < 2.6$ in order to characterize changes that are taking place in Mg II selected structures over a large span of cosmic time.

6. Use synthetic quasar spectra generated from cosmological hydrodynamic n-body galaxy formation models to constrain the simulation parameters.

All of these distributions will be compared for different redshift bins and at various equivalent width cutoffs in order to trace changes in the absorbing gas.

3. DATA

We currently have about 200 HIRES/Keck and UVES/VLT quasar absorption line spectra, which is the largest known sample of such high quality spectra. An example is shown in Figure 1. The spectral resolution is $R = 45,000$, or ~ 6.6 km/s, and the spectra have three pixels per resolution element. The signal-to-noise ratios are typically 25 - 80. The redshift coverage of the survey is $0.2 < z < 2.6$, and is illustrated in Figure 2.

The HIRES spectra were provided by Charles Steidel (Caltech), Jason Prochaska (UCSC), Christopher Churchill (NMSU), Wallace Sargent (Caltech), and Michael Rauch (Carnegie). The UVES spectra were provided by Michael Murphy (Swinburne). The spectra of Churchill and Steidel were selected for Mg II absorption (Churchill & Vogt 2001; Churchill et al. 2003; Steidel et al. 2002) and were based upon previous studies which used low resolution spectra to detect Mg II absorption of equivalent width $W_r(2796) \geq 0.3$ Å (Sargent et al. 1988; Steidel & Sargent 1992). Those of Sargent and Rauch were selected for high resolution analysis of Ly α forest and C IV absorption, and those of Prochaska for damped Lyman alpha (DLA) absorption (Prochaska et al. 2007). The spectra of Murphy were drawn from the UVES/VLT archive, and were obtained by several researchers for various purposes, including Ly α forest, Mg II, C IV, O IV, and DLA studies. The spectra of Churchill were reduced using standard IRAF reduction (see Churchill 1997); those of Sargent, Rauch, Prochaska, and Steidel were reduced using the MAKEE software package of Barlow (2005); and the spectra of Murphy were reduced using the UVES pipeline and post-processed using the UVES_popler software package [see Dekker et al. (2000) and Murphy (2008) respectively]. All the spectra have been corrected to heliocentric vacuum velocities.

Since some of the spectra were taken because the presence of strong Mg II absorption had already been ascertained, the sample is only unbiased for weak systems, which have $W_r(2796) < 0.3$ Å. The early studies that discovered the existence of strong Mg II absorbers did not have the sensitivity to detect weak absorbers.

4. Analysis

4.1. Identifying Doublets

Using the program SEARCH1, the spectra are objectively searched for Mg II doublet candidates. The initial criteria are the detection of a 5 σ feature, which is taken to be the λ2796 line, along with a corresponding 3 σ detection for the λ2803 feature. Detections and significance levels follow the formalism of Schneider et al. (1993). The candidate doublets are then checked for appropriate doublet ratios of $1.0 \leq DR \leq 2.0$, and their line profiles are visually inspected to determine whether they are consistent with each other and eliminate any spurious features. Two or more Mg II features are considered to be a single system if they lie within $\leq$ 800 km/s of each other. The candidates are also checked for corresponding absorption in the following transitions: Mg I λ2853; Fe II λ2344, λ2374, λ2383, λ2587, and λ2600; the Ca II $\lambda\lambda$3935, 3970 doublet; and Mn II λ2577, λ2594, and λ2606.

Once the presence of Mg II is confirmed, the equivalent widths, velocity centroids, velocity spreads, and upper and lower velocity limits are determined for both the whole system and for the kinematic subsystems using the program SYSANAL. All quantities are calculated for the Mg II, Mg I, Fe II, Mn II, and Ca II transitions and limits. Kinematic subsystems are regions of detected absorption separated by regions of no detected absorption, but which are close enough together in velocity space that they are considered a single system. Figure 3 shows two Mg II systems. The largest system spans the region marked by the arrows and consists of five kinematic subsystems; the smaller system lies $\sim$ 1000 km/s away. SYSANAL also generates optical depth spectra and equivalent width limit spectra for each system. Then AUTOVP (written by Romeel Davé and modified by Churchill to include instrumental spread function convolution) automatically creates an initial model of the system's VP components. With the graphical interactive program IVPFIT, the user can adjust this initial input model to fit the data as closely as possible. Finally, MINFIT (Churchill 1997) takes this initial model of VP components, eliminates all statistically insignificant components, and adjusts the remaining components to minimize χ^2. The code outputs the velocities, column densities, Doppler b parameters, and temperatures of the system components.

4.2. Direct Flux Measurements

Studying the system rest frame equivalent width distribution tells us about the nature of Mg II absorption. We are able to detect systems down to $W_r(2796) < 0.02$ Å. The equivalent width of a Mg II system results from both the column density of its components and its kinematics - i.e. the manner in which the components are distributed in velocity space. The

rest frame equivalent width of an absorption line is equal to

$$W_r = \frac{W_{obs}}{(1+z)} \tag{1}$$

where W_{obs} is the observed equivalent width:

$$W_{obs} = \int_{\lambda_1}^{\lambda_2} \left(1 - \frac{I}{I_c}\right) d\lambda \tag{2}$$

and where λ_1 and λ_2 are the wavelength limits of the feature, I is the flux at wavelength λ and I_c is the continuum flux at that wavelength.

The distribution of absorber equivalent widths can be fit with a power law or an exponential. Nestor et al. (2005), using a large Sloan Digital Sky Survey sample, found that the distribution for $W_r(2796) \geq 0.02$ Å was fit best by a two-component exponential. Narayanan et al. (2007) found evidence for a turnover in the equivalent width distribution for the weakest absorbers ($W_r(2796) < 0.1$ Å), although they did not correct for survey incompleteness at these small equivalent widths. We will examine whether there is truly some characteristic turnover value below which systems decrease in frequency, or whether equivalent widths continue to follow a power law down to the weakest observable systems. It is also useful to compare the distribution at different redshifts to study the weak absorber evolution (see § 4.4).

The output of SYSANAL also allows us to construct distributions of the velocity spreads of the systems and of the apparent optical depth (AOD) column densities. These must be compared for different equivalent width cutoffs and, like the equivalent width distribution, for different redshift bins to analyze evolution.

Another useful quantity is the flux decrement per pixel of an absorption system. Comparing the distributions of flux decrements per pixel for different redshift bins and equivalent width cutoffs provides information about the relative system optical depths and how these have changed through cosmic time. We can also segregate the flux decrements by kinematics (i.e. bin by the velocity of the pixels) to examine evolution with redshift.

4.3. Voigt Profile Analysis

The process of VP modeling is begun by using AUTOVP to produce an initial model of the components of an absorption system. The code assigns each component it finds a velocity, column density, and Doppler b parameter. Then with IVPFIT the user can interactively alter these parameters for each component, as well as add additional components as

deemed necessary, to create an input model for MINFIT. MINFIT finds the least squares fit for each component's parameters as well as discards any components that are not statistically significant using the F-test, so that only the smallest number of components that can accurately model the system remain. This code yields the final number of components and their velocities, column densities, and Doppler b parameters. An example of a VP model plotted over the data is shown in Figure 4.

The column density N of each Mg II absorber is obtained from the VP fits of its component clouds. The column density distribution can be studied in a manner similar to that of the equivalent widths using a power law fit. This quantity can sometimes be more revealing because, though more difficult to obtain because of the need to VP model, it can somewhat account for saturation and therefore the differing sizes of systems that might lie on the flat part of the curve of growth.

The Doppler b parameter is a measure of the line broadening. Assuming pure thermal broadening, the b parameter is

$$b_{therm} = \sqrt{\frac{2kT}{m}} \tag{3}$$

where k is Boltzmann's constant, T is the temperature of the absorbing gas, and m is the mass of the absorbing species. Thus, extracting the Doppler parameters via Voigt profile analysis yields information about the temperature conditions under which Mg II absorption occurs. When a turbulent component to the gas motion is assumed, the b parameter becomes:

$$b^2 = b_{therm}^2 + b_{turb}^2. \tag{4}$$

The velocity two-point correlation function (TPCF) is the probability that any randomly selected pair of VP components in a system will have a particular velocity difference. Petitjean & Bergeron (1990); Churchill et al. (2003) fit their TPCF distributions using two-component Gaussian models.

In a sample of strong systems, the Churchill et al. study, which had superior spectral resolution and drew upon more lines of sight, found that the components of the best fit had dispersions of 54 km/s and 166 km/s. This suggests that there are two distinct kinematic phenomena giving rise to the absorption.

4.4. Evolution of Weak MgII Absorbers

Redshift Number Density

Since this survey is unbiased for weak MgII absorption and has the sensitivity to detect systems down to $W_r(2796) < 0.02$ Å, the evolution of these systems with cosmic time can be studied. The redshift number density is the number of absorbers per unit redshift, dN/dz. It is a key quantity in determining whether the number of MgII systems is evolving, which in turn can yield clues about galaxy evolution.

In practice dN/dz is determined for a set of redshift bins:

$$\frac{dN}{dz}_i = \frac{N_{abs,i}}{\Delta Z_i(W_r)} \tag{5}$$

where $N_{abs,i}$ is the number of absorbers in redshift bin i having rest equivalent widths greater than some cutoff W_r, and $\Delta Z_i(W_r)$ is the cumulative redshift path length within that redshift bin for the same equivalent width cutoff. The cumulative redshift path $Z(W_r)$ is the total redshift coverage of the survey as a function of some minimum rest frame equivalent width. It can be expressed as

$$Z(W_r) = \int_{z_1}^{z_2} g(W_r, z) dz \tag{6}$$

where $g(W_r, z)$ is the redshift sensitivity function. The dependence of the cumulative redshift path on W_r is useful in considering the completeness of the survey; for instance, a survey might be 100% complete at $W_r \geq 3.0$ Å, but only 90% complete at $W_r \geq 0.02$ Å. This would mean that a system of rest equivalent width 0.02 Å could only have been detected in 90% of the total spectral coverage.

The redshift sensitivity function $g(W_r, z)$ is the number of lines of sight along which an absorption feature with rest frame equivalent width of at least W_r and at redshift z could have been detected. The sensitivity function must be taken into account particularly to study the weak systems, since there is a certain equivalent width cutoff at any given point in a spectrum below which the weakest systems are lost in the noise. The redshift sensitivity function (see Lanzetta et al. 1987; Steidel & Sargent 1992) of the jth rest equivalent width and kth redshift interval can be written

$$g(W_{r,j}, z_k) = \sum_n H(z_k - z_{min,n}) H(z_{max,n} - z_k) H(W_{r,j} - N_\sigma \sigma_{W,k}) \tag{7}$$

where H is the Heaviside step function; n is the index of the QSO; $z_{min,n}$ is the redshift of either the observed wavelength of the Lyα emission or the shortest observed wavelength, whichever is larger; $z_{max,n}$ is the redshift of either the wavelength corresponding to 5000 km/s

blueward of the Mg II emission or the longest observed wavelength, whichever is smaller; N_σ is the significance level of the detection; and $\sigma_{W,k}$ is the detection limit. H is defined as being equal to 1 when its argument is nonnegative and 0 when its argument is negative. The function $g(W_r, z)$ reveals over which equivalent widths and redshifts the survey is most sensitive.

The redshift number density can be parameterized as:

$$\frac{dN}{dz} = \frac{c}{H_0} n_0 \sigma_0 \frac{(1+z)^{2+\epsilon}}{\sqrt{\Omega_m (1+z)^3 + \Omega_\Lambda}} \tag{8}$$

where n_0 is the number density of absorbers, σ_0 is the geometric absorber cross section, and ϵ is an evolution parameter, where $\epsilon = 0$ would represent the no-evolution expectation for the product $n(z)\sigma(z)$. By assuming a cosmological model, and using the maximum-likelihood method to determine the best-fit value of ϵ, the behavior of dN/dz with redshift can be studied and compared to the no-evolution expectation. Narayanan et al. (2007) found evolution in dN/dz for weak absorbers. The redshift number density was found to peak at a redshift of 1.2 with a value of 1.76 ± 0.08. This implies that the absorber number density and/or cross section are evolving with redshift.

4.5. High Redshift and Low Redshift Subsamples

To begin to examine the evolution of Mg II absorbers, for a preliminary analysis, I divided my sample into the following redshift bins: $0.2 \leq z < 0.6$, $0.6 \leq z < 1.5$, and $1.5 \leq z < 2.6$, which I refer to as the low, middle and high redshift bins, respectively. The cumulative equivalent width distributions for these three subsamples are shown in Figure 5. In the low redshift sample, there are relatively more small equivalent width systems; however, the difference between the high and the low redshift populations is only significant at a 91% confidence level.

To determine why the equivalent distribution might be evolving, we can analyze the flux decrement per pixel distributions as in Figure 6, where they have been plotted for four different equivalent width cutoffs of $W_r(2796) \geq 0.02$ Å, $W_r(2796) \geq 0.3$ Å, $W_r(2796) \geq 0.6$ Å, and $W_r(2796) \geq 1.0$ Å. Here there is highly statistically significant evolution between the low and high redshift populations, to a greater than 99.99% confidence level. The low redshift sample is very distinct from the other redshift bins at all equivalent width cutoffs. However, the redshift evolution becomes most pronounced when only the strongest systems are considered, i.e. the highest cutoff is applied (see Steidel & Sargent 1992; Nestor et al. 2005). This means the optical depths of the strongest Mg II absorbers are decreasing toward

the present. There seems to be some process whereby these systems are becoming smaller, possibly being torn apart into optically thinner clouds.

Another interesting point can be noted concerning the flux decrements for $W_r(2796) \geq 0.02$ Å, which includes nearly the entire absorber sample. The greatest flux removal per pixel occurs in the middle redshift bin of $0.6 \leq z < 1.5$ as compared to the low and high redshifts. That this effect occurs only at the lowest equivalent width cutoff means that it is indicative of the changing optical depths of the weakest absorbers: they seem to have peaked at some point in the middle redshifts.

Figure 7 shows the evolution in the total velocity width distribution of the systems. Here the total velocity width is defined as the difference between the velocity extrema of the entire system, $v^+ - v^-$. The lowest redshift systems are systematically narrower than the middle and high redshift populations, and their velocity widths do not exceed ~ 400 km/s, whereas the higher redshift systems can occasionally have velocity widths in excess of 1000 km/s. The kinematic difference between the populations at low and high redshift illustrates that it is not only decreasing optical depths, but also a tendency to become narrower in velocity space toward the present, that contributes to the evolution in the MgII equivalent widths. The systematic decrease in velocity widths indicates a general trend toward less kinematically complex MgII absorbing gas.

5. SIMULATIONS

The ΛCDM cosmological simulations were performed in a $10h^{-1}$ Mpc $\times$ $10h^{-1}$ Mpc comoving box using the Eulerian Gasdynamics plus N-body Adaptive Refinement Tree (ART) code (Kravtsov et al. 1997; Kravtsov 1999; Kravtsov & Klypin 1999; Kravtsov et al. 2004). The initial conditions are a set of small density fluctuations at $z = 50$. The model uses $\Omega_m = 0.3$, $\Omega_\Lambda = 0.7$, $h = 0.7$, and $\sigma_8 = 0.9$. An adaptive mesh method is implemented so that there exist regions of varying spatial resolution, depending on what is needed (based on the dynamical timescales of the physics in a given location within the simulation). The gas cells are 50 - 200 pc in size, with resolution decreasing toward lower redshift. The code includes star formation, feedback from type Ia and II supernovae, cooling and heating, and ionizing ultraviolet background.

5.1. Synthesis of Spectra

To create synthetic quasar absorption line spectra, a grid of lines of sight is constructed through the simulation box using the code LOS4; all of the cells intercepted by a line of sight are taken into account when constructing the corresponding spectrum. For my preliminary experiment, I used a face-on grid extending ± 100 kpc from the galaxy center in the x and y directions, with lines of sight at 10 kpc intervals. To generate the spectra from the intercepted gas cells, the code SPECSYNTH is used.

5.2. Analysis

The analysis of the simulated spectra will be conducted using the same methods, search algorithm, and analysis and VP modeling codes as for the observational data. Treating both data sets in a uniform manner will ensure that they can be compared meaningfully.

The simulations will yield the equivalent widths, column densities, Doppler b parameters, kinematic information, and other properties just as were extracted from the actual spectra. The evolution in these quantities can also be measured since the simulations are run down to $z = 0$.

6. COMPARISON OF DATA WITH SIMULATIONS

Using my preliminary sample of synthetic quasar lines of sight as described in § 5.1, I analyzed these data over the redshift range $0.6 \leq z < 1.5$ and compared them to the observational data within the same redshift bin. Figure 8 shows that the simulations do not reproduce the observed equivalent width distribution. The simulated spectra yield relatively too many low equivalent width systems.

To explore the reason for this discrepancy, we can compare both the flux decrement per pixel distributions and the total velocity width distributions. Figure 9 shows that the flux decrements in the simulation sample are too weak, i.e. there is a tendency for the Mg II systems to have lower optical depths than those in the observational sample. In Figure 10 we can also see that there is a dramatic difference in the velocity widths of the two populations. The simulations produce absorbers that are systematically too narrow.

This simulation work has just begun, and would be expanded to include more inclination angles and other galaxies to obtain a most robust sample for comparison to the observations. The preliminary result is that the Mg II absorption produced tends to be too weak. There is

the possibility that both the deficient column densities and the kinematic quiescence could be remedied by altering the stellar feedback prescription as discussed in § 1. Although the simulations do not yet seem to be reproducing observations, there is great potential for using the synthetic quasar absorption line spectra to probe the kinematics and structure of gas in and around galaxies.

7. TIMELINE

Summer 2008

- Combine multiple spectra of the same quasar into optimally combined single spectra
- Search and reanalyze these along with any remaining UVES spectra that have been added to the archive

Summer/Fall 2008

- Complete Voigt profile fitting of systems (all weak systems and some of the strong systems are already fit)

Fall 2008

- Analyze the redshift path coverage and dN/dz using three different techniques
- Construct distributions and perform statistical tests on data to determine best fit parameters

Winter 2008

- Begin writing large data paper (there may be more than one)

Spring 2009

- Submit data paper

Spring/Summer 2009

- Finalize design of simulation experiment to best emulate observational selection effects

Summer 2009

- Complete analysis of simulation data
- Begin writing simulation paper (there may be more than one)

Fall 2009

- Submit simulation paper
- Begin applying to jobs

Winter 2009

- Begin third paper

Summer 2010

- Submit paper
- Defend dissertation

REFERENCES

Barlow, T. 2005, MAKEE software package, www2.keck.hawaii.edu/inst/hires/data_reduction.html

Bond, N. A., Churchill, C. W., Charlton, J. C., & Vogt. S. S. 2001, ApJ, 557, 761

Bond, N. A., Churchill, C. W., Charlton, J. C., & Vogt. S. S. 2001, ApJ, 562, 641

Charlton, J. C., & Churchill, C. W. 1998, ApJ, 499, 181

Charlton, J. C., Churchill, C. W., Ding, J., Zonak, S., Bond, N., & Rigby, J. R. 2002, ASPC, 254, 122

Churchill, C. W. 1997, Ph.D. thesis, University of California, Santa Cruz

Churchill, C. W., Rigby, J. R., Charlton, J. C., & Vogt, S. S. 1999, ApJS, 120, 51

Churchill, C. W., & Vogt, S. S. 2001, ApJ, 112, 679

Churchill, C. W., Vogt, S. S., & Charlton, J. C. 2003, ApJ, 125, 98

Dekker, H., D'Odorico, S., Kaufer, A., Delabre, B., & Kotzlowski, H. 2000, SPIE, 4008, 534

Kacprzak, G. G., Churchill, C. W., Steidel, C. C., & Murphy, M. T. 2008, AJ, 135, 922

Kravtsov, A. V. 1999, Ph.D. thesis, New Mexico State University

Kravtsov, A. V., Gnedin, O. Y., & Klypin, A. A. 2004, ApJ, 609, 482

Kravtsov, A. V., & Klypin, A. A. 1999, ApJ, 520, 437

Kravtsov, A. V., Klypin, A. A., & Khokhlov, A. M. 1997, ApJS, 111, 73

Lanzetta, K. M., Turnshek, D. A., & Wolfe, A. M. 1987, ApJ, 332, 739

Lynch, R. S., & Charlton, J. C. 2007, ApJ, 666, 64

Milutinović, N., Rigby, J. R., Masiero, J. R., Lynch, R. R., Palma, C., Charlton, J. C. 2006, ApJ, 641, 190

Murphy, M. T. 2008, UVES_popler software package, astronomy.swin.edu.au/~mmurphy/UVES_popler

Narayanan, A., Misawa, T., Charlton, J. C., & Kim, T. 2007, ApJ, 660, 1093

Nestor, D. B., Turnshek, D. A., & Rao, S. M. 2005, ApJ, 628, 637

Petitjean, P., & Bergeron, J. 1990, A&A, 231, 309

Prochaska, J. X., Wolfe, A. M., Howk, J. C., Gawiser, E., Burles, S. M., & Cooke, J. 2007, ApJS, 171, 29

Sargent, W. L. W., Steidel, C. C., & Boksenberg. A. 1988, ApJ, 334, 22

Schneider, D. P. et al. 1993, ApJS, 87, 45

Steidel, C. C., Dickinson. M., & Persson, S. E. 1994, ApJ, 437, 75

Steidel, C. C. 1995, in ESO Astrophysics Symp., QSO Absorption Lines, ed. G. Meylan, (Berlin: Springer-Verlag), 139

Steidel, C. C., Kollmeier, J. A., Shapley, A. E., Churchill, C. W., Dickinson, M., & Pettini, M. 2002, ApJ, 570, 526

Steidel, C. C., & Sargent, W. L. W. 1992, ApJS, 80, 1

Tripp, T. M., & Bowen, D. V. 2005 in IAU Colloquia 199, Probing Galaxies through Quasar Absorption Lines, ed. P. R. Williams, C. Shu &B. Ménard (Cambridge: Cambridge University Press), 5

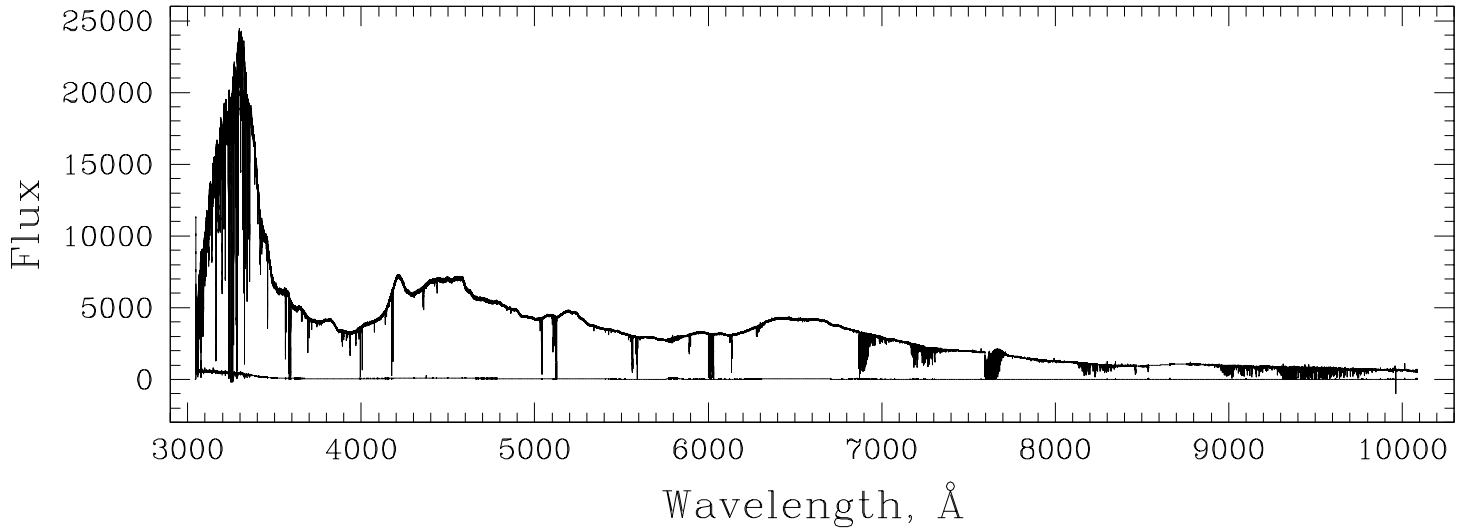

Fig. 1.— An example of the sample, the UVES spectrum HE0515m4414, and its uncertainty spectrum.

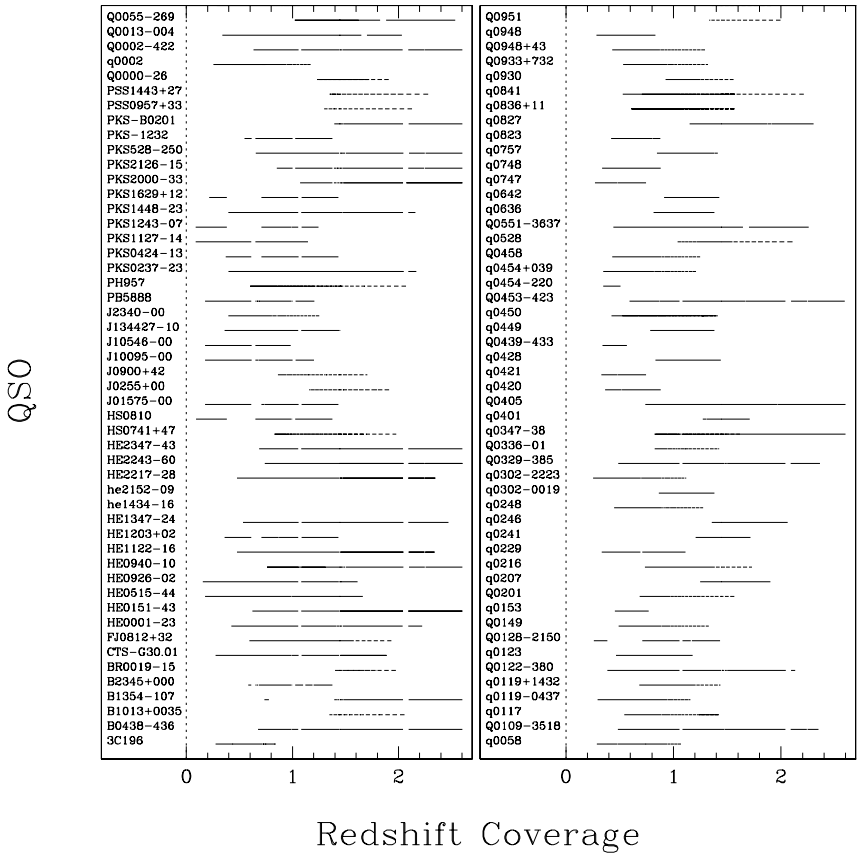

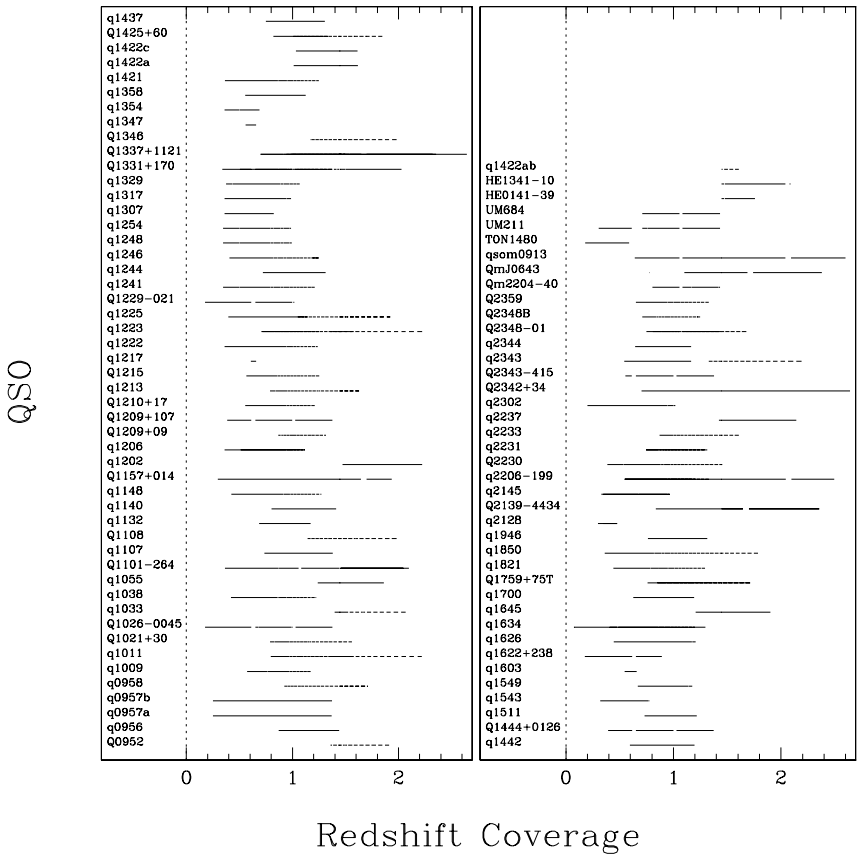

Fig. 2.— The redshift coverage of each quasar spectrum in the sample.

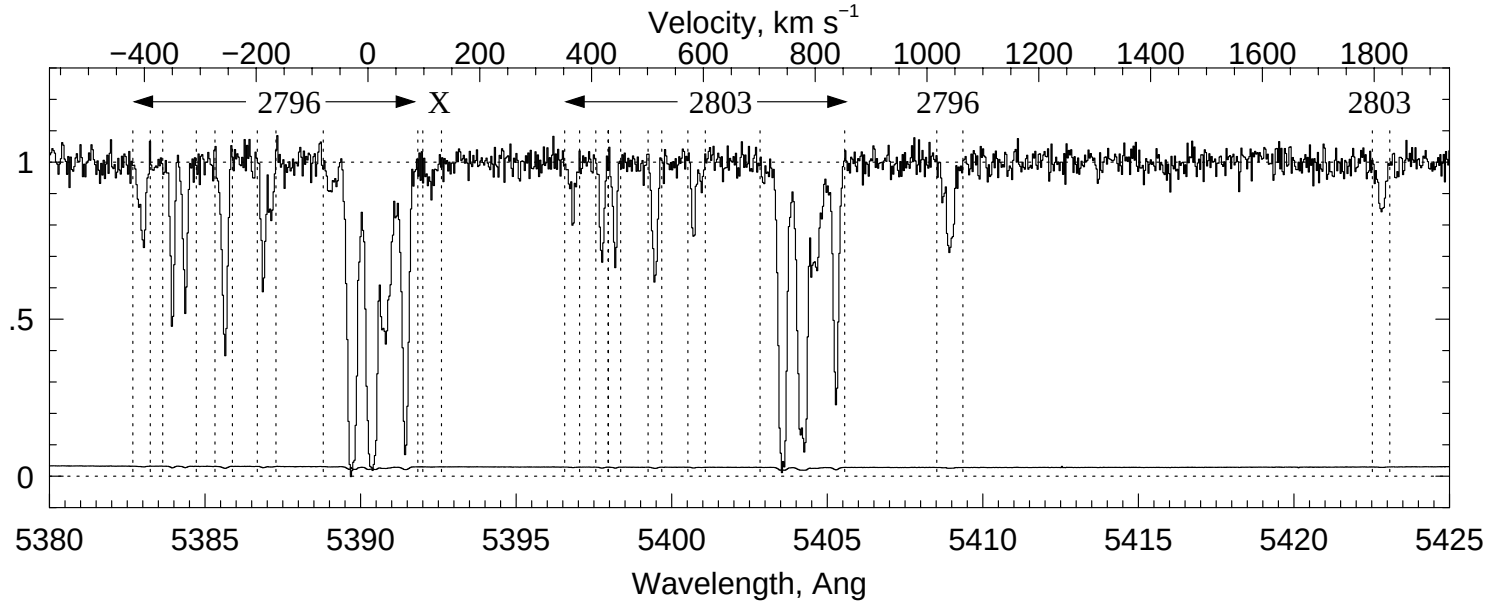

Fig. 3.— An example of a Mg II $\lambda\lambda 2796, 2803$ doublet with several kinematic subsystems. The $\lambda 2796$ feature at ~ 1000 km/s and its corresponding $\lambda 2803$ feature at ~ 1800 km/s are considered a separate system since they lie ≥ 800 km/s away from the other features. The feature marked with an "X" is not part of the Mg II system.

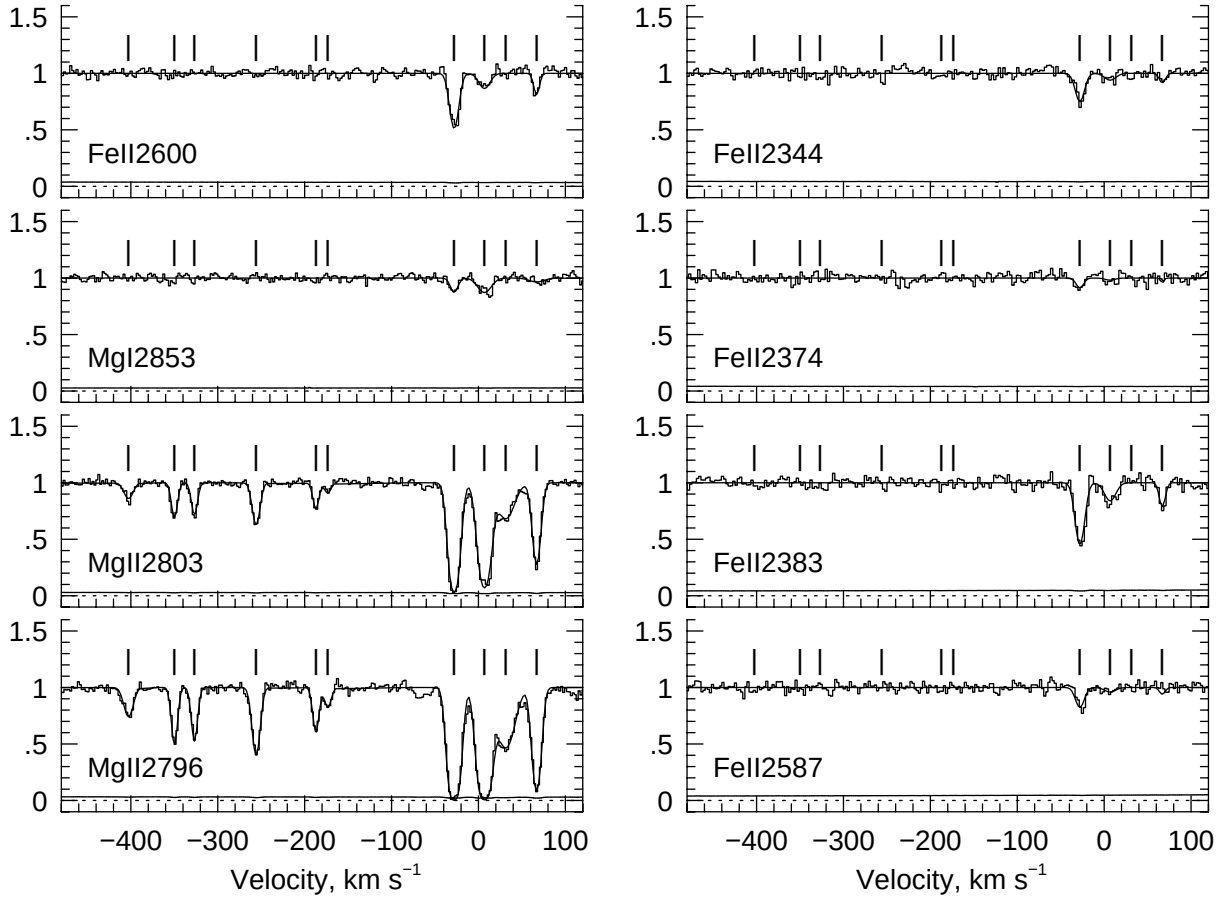

Fig. 4.— A Voigt profile model of the MgII and FeII lines of an absorbing system.

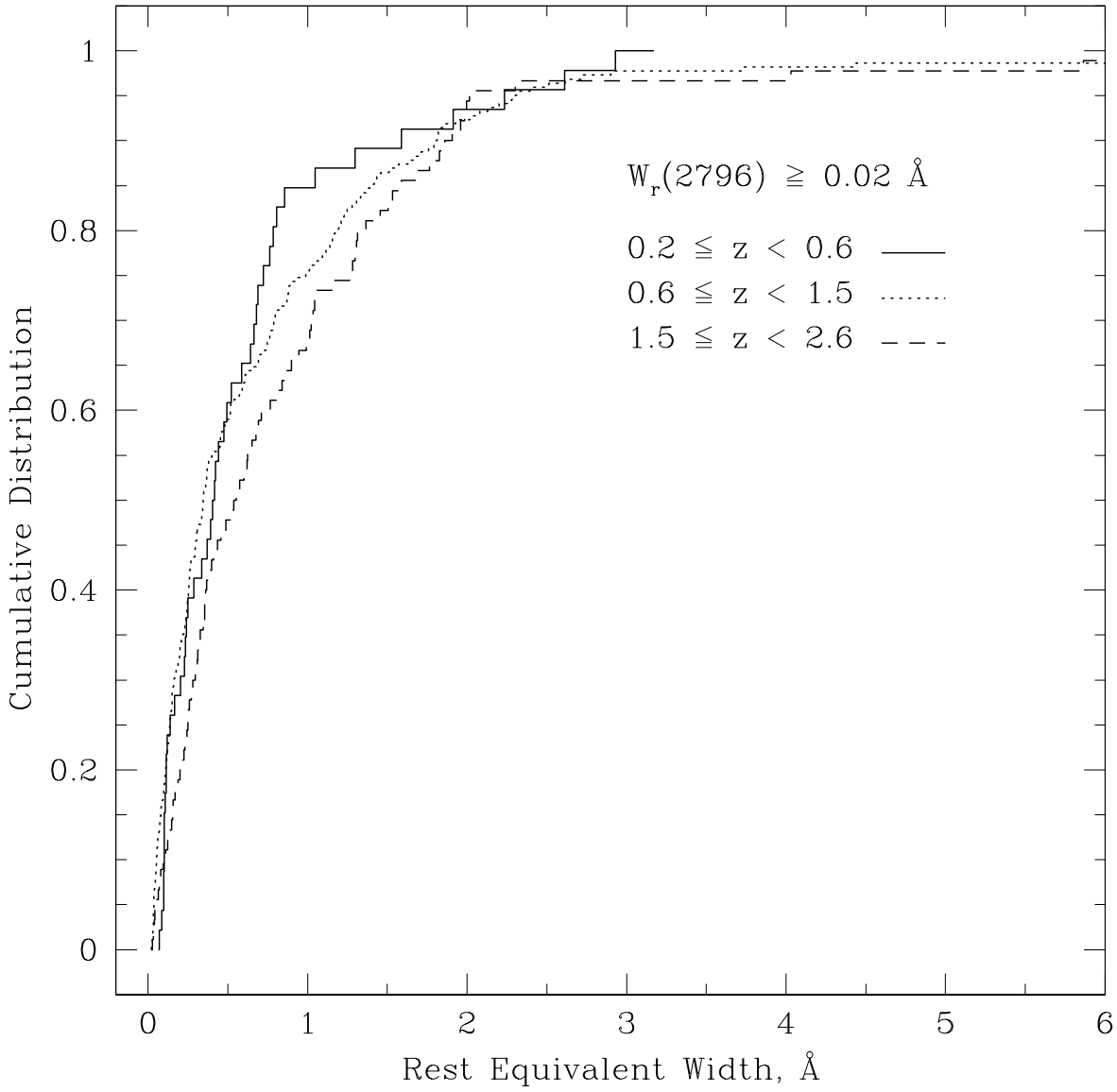

Fig. 5.— The cumulative rest equivalent width distributions of all Mg II absorbers with $W_r(2796) \geq 0.02$ Å, divided into redshift bins as indicated by the solid, dotted, and dashed lines. The high and low redshift bins are statistically different to a 91% confidence level.

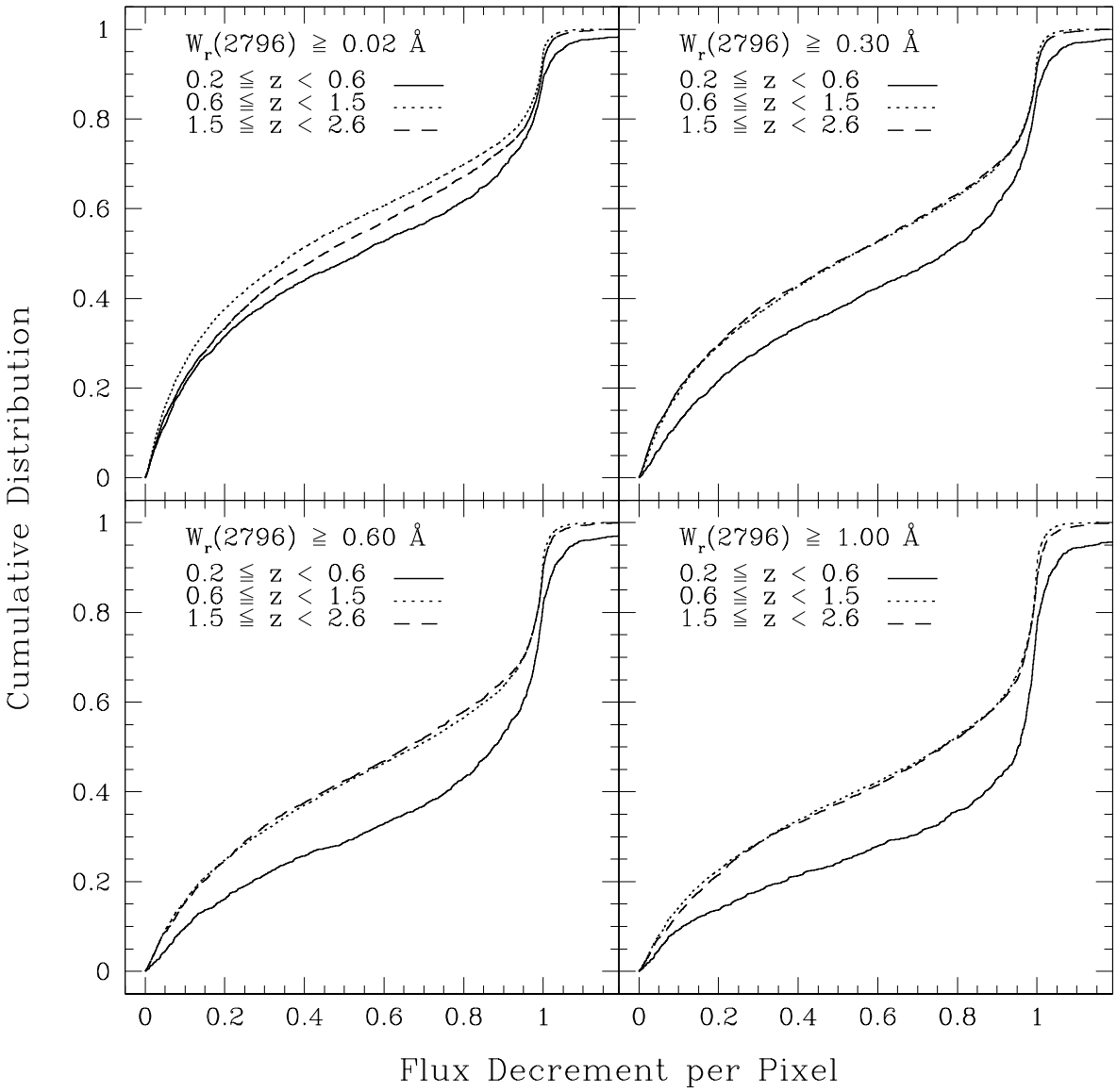

Fig. 6.— The cumulative distributions of flux decrements per pixel for Mg II systems at four equivalent width cutoffs $W_r(2796)$, divided into redshift bins indicated as in Figure 5. The equivalent width cutoff is increasing going from the upper left panel to the lower right panel. The high and low redshift bins are statistically different to a greater than 99.99% confidence level for all four cutoffs.

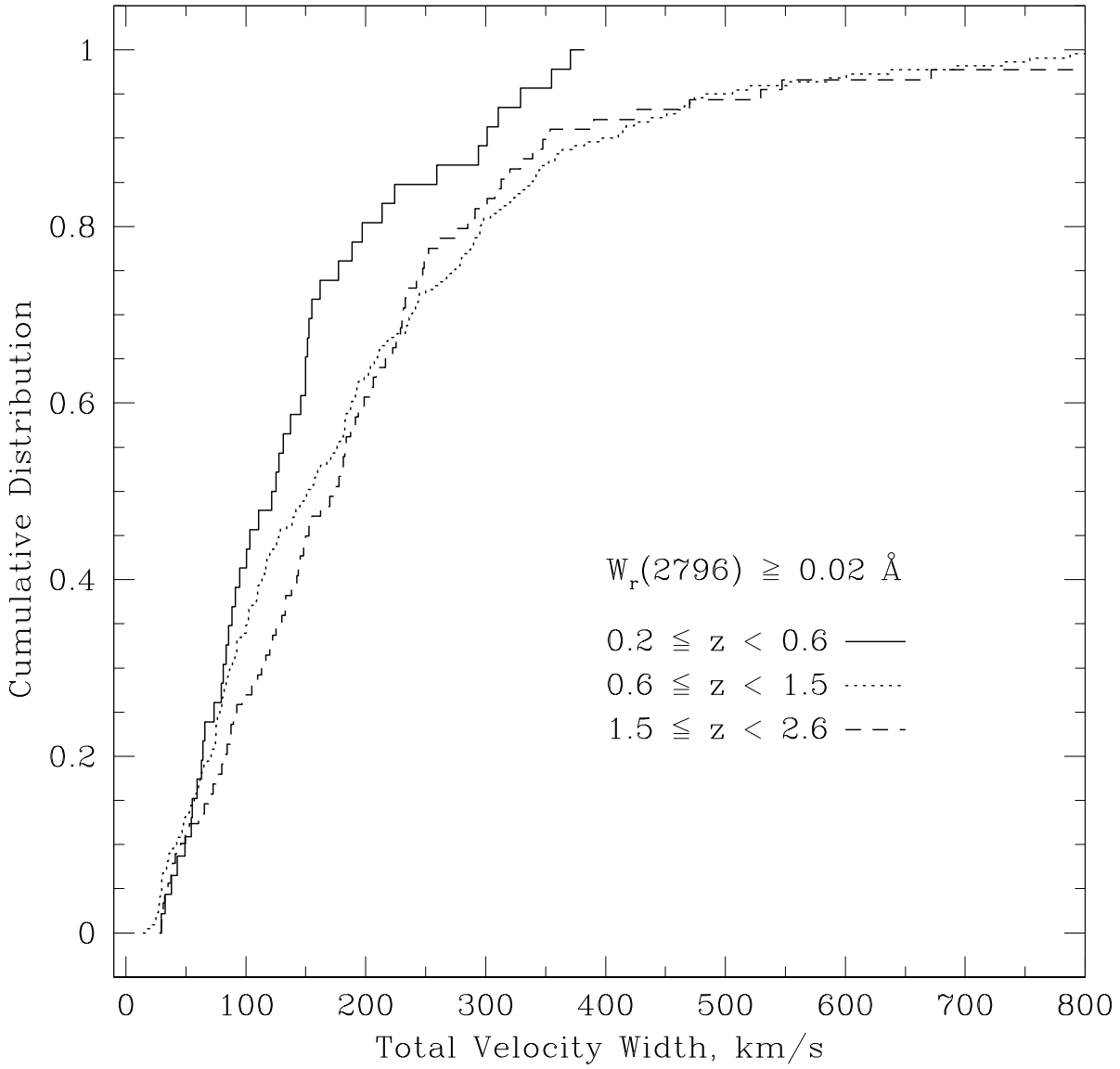

Fig. 7.— The cumulative distributions of system total velocity widths for $W_r(2796) \geq 0.02$ Å, divided into redshift bins indicated as in Figure 5. The high and low redshift bins are statistically different to a 98% confidence level.

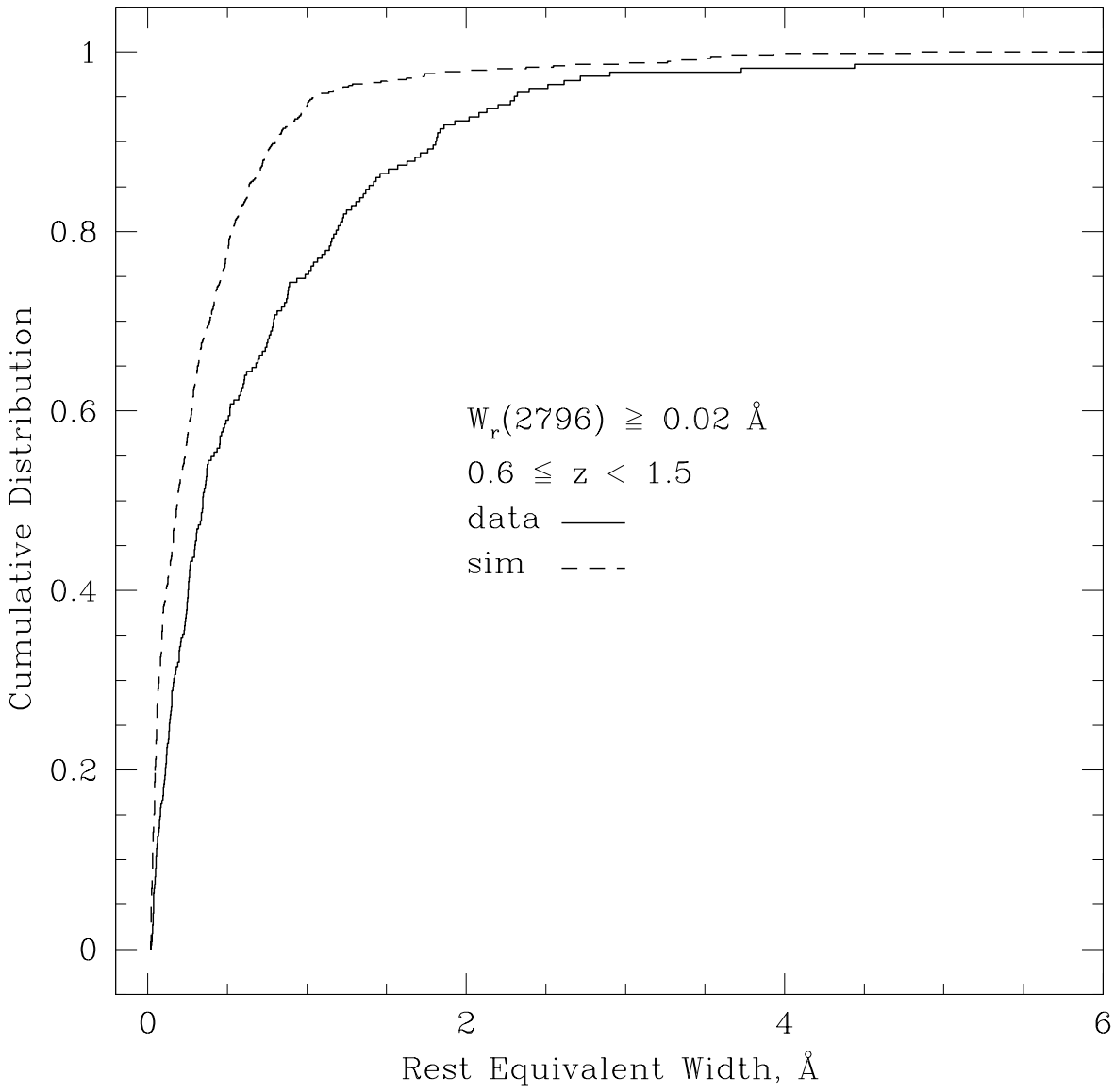

Fig. 8.— The cumulative equivalent width distributions for $W_r(2796) \geq 0.02$ Å and $0.6 \leq z < 1.5$ for both the data (solid) and simulation (dashed) samples.

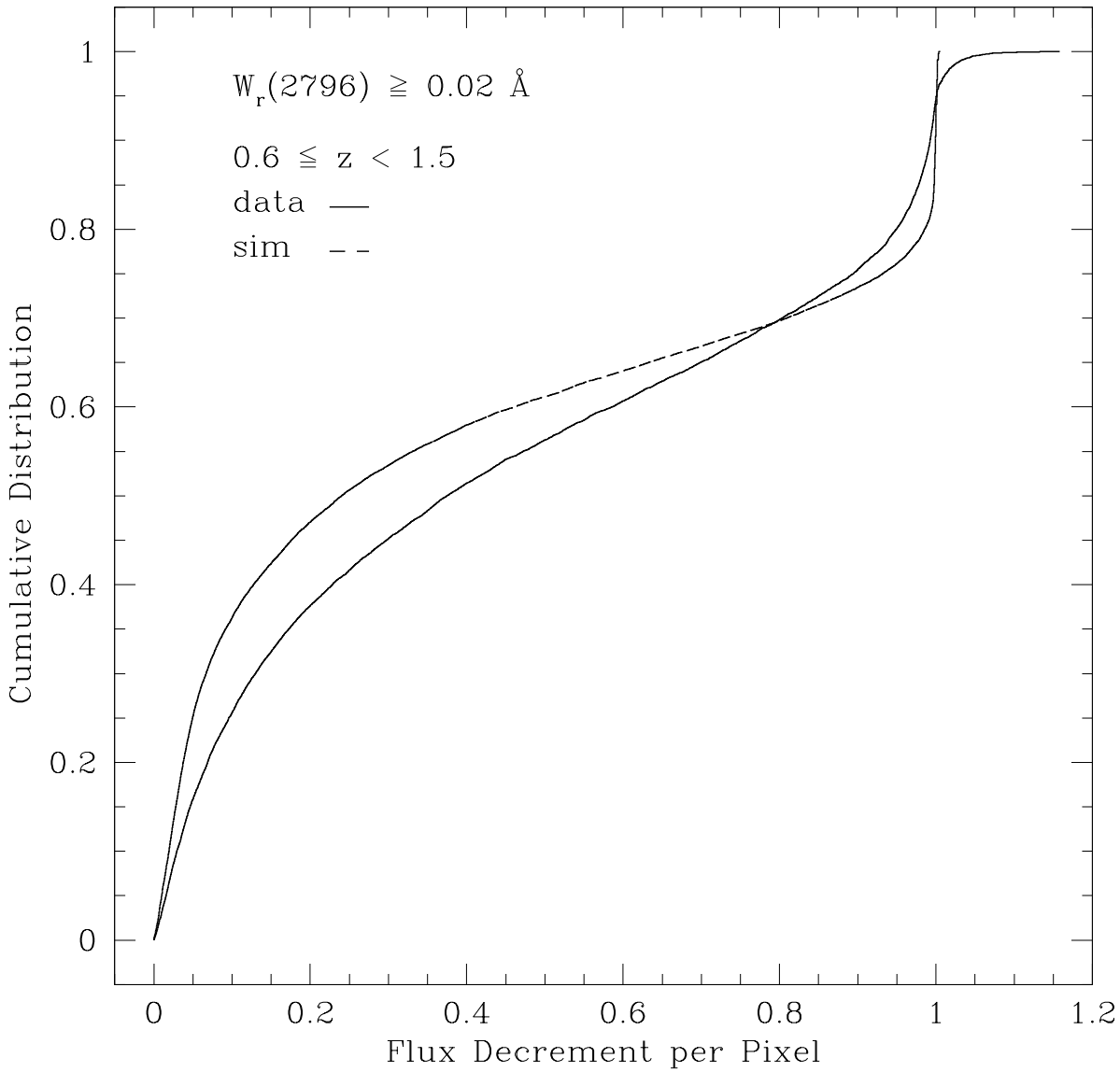

Fig. 9.— The cumulative distributions of flux decrements per pixel for $W_r(2796) \geq 0.02$ Å and $0.6 \leq z < 1.5$ for both the data (solid) and simulation (dashed) samples.

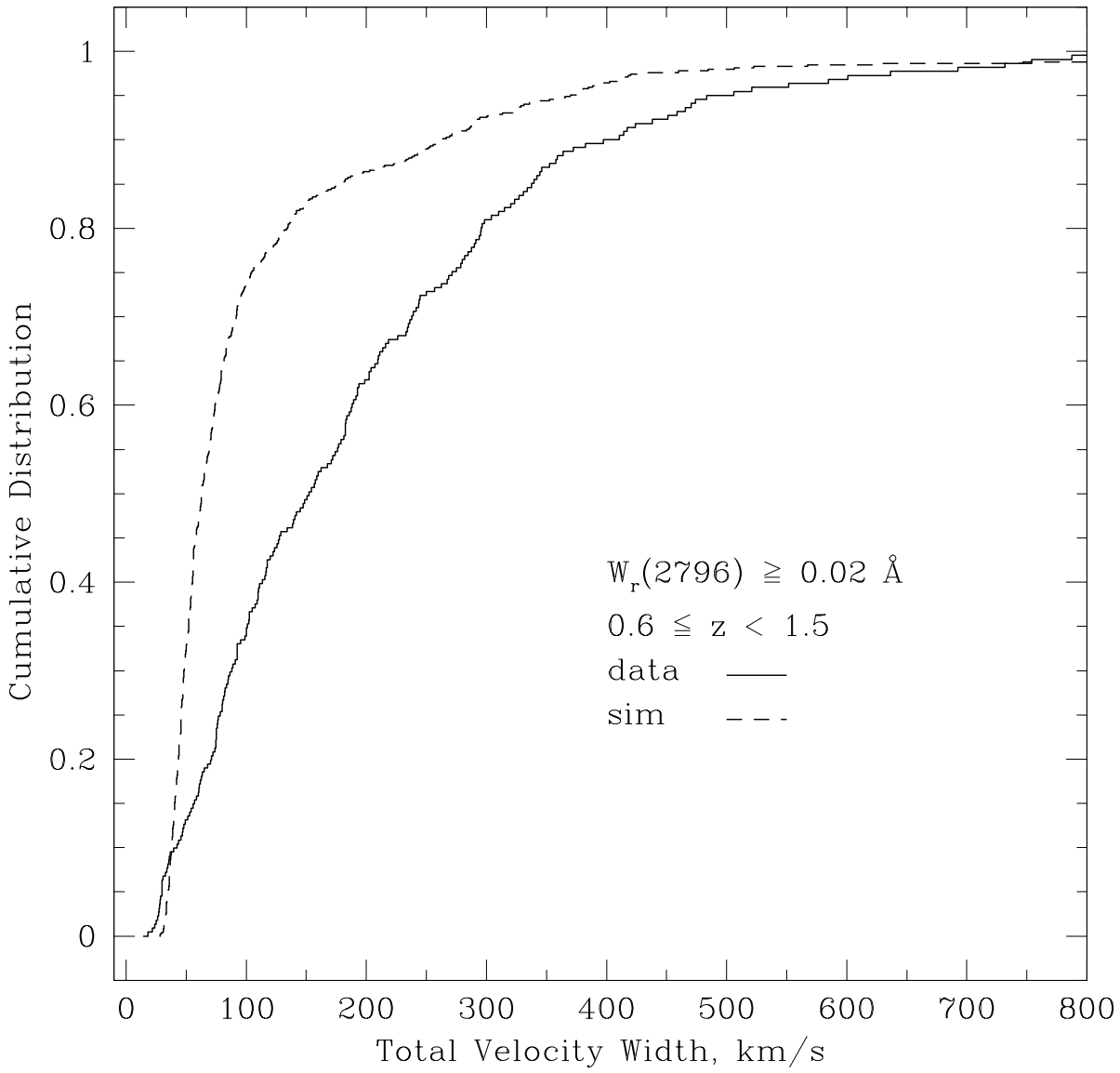

Fig. 10.— The cumulative distributions of system total velocity widths for $W_r(2796) \geq 0.02$ Å and $0.6 \leq z < 1.5$ for both the data (solid) and simulation (dashed) samples.